nature neuroscience

Coactivation of thalamic and cortical pathways induces input timing–dependent plasticity in amygdala

Jun-Hyeong Cho[1], Ildar T Bayazitov[2], Edward G Meloni[1], Karyn M Myers[1], William A Carlezon Jr[1], Stanislav S Zakharenko[2] & Vadim Y Bolshakov[1]

Long-term synaptic enhancements in cortical and thalamic auditory inputs to the lateral nucleus of the amygdala (LAn) mediate encoding of conditioned fear memory. It is not known, however, whether the convergent auditory conditioned stimulus (CSa) pathways interact with each other to produce changes in their synaptic function. We found that continuous paired stimulation of thalamic and cortical auditory inputs to the LAn with the interstimulus delay approximately mimicking a temporal pattern of their activation in behaving animals during auditory fear conditioning resulted in persistent potentiation of synaptic transmission in the cortico-amygdala pathway in rat brain slices. This form of input timing–dependent plasticity (ITDP) in cortical input depends on inositol 1,4,5-trisphosphate ($InsP_3$)-sensitive Ca^{2+} release from internal stores and postsynaptic Ca^{2+} influx through calcium-permeable kainate receptors during its induction. ITDP in the auditory projections to the LAn, determined by characteristics of presynaptic activity patterns, may contribute to the encoding of the complex CSa.

The LAn is a brain structure that integrates conditioned and unconditioned stimuli (UCS) during fear conditioning[1,2]. Both cortical and thalamic inputs, arising from the auditory cortex and the auditory thalamus, respectively, deliver CSa information to the LAn and support fear learning[3]. It has been suggested, however, that these two routes for CSa delivery could differ in their contributions to the acquisition of fear memory in the intact brain[4]. Thus, the cortical areas contribute more substantially to the processing of complex CSa[5]. Signals transmitted by direct projections from the auditory thalamic areas reach the LAn earlier than those arriving from the auditory cortex[6–9]. Consistent with the role of behaviorally induced plasticity in the direct thalamo-amygdala pathway in fear learning, fear conditioning was found to be associated with substantial enhancements of the short-latency auditory responses, reflecting inputs from the auditory thalamus, in LAn neurons in freely moving rats[8]. Subsequent findings provided extensive evidence that the mechanisms of long-term potentiation (LTP) in both cortico- and thalamo-amygdala pathways could mediate memory of the CSa-UCS association during fear conditioning[10–14].

The ability of synapses in both thalamic and cortical inputs to undergo LTP independently[15] likely reflects the sufficiency of either projection for fear learning[3]. Nevertheless, on the basis of results of the experiments in freely moving rats, it has been suggested that associative interactions between two auditory inputs to the LAn could lead to the mutual synaptic strengthening in the CSa pathways[16]. However, synaptic mechanisms of such potential interactions between convergent thalamic and cortical inputs to the LAn have not been explored. We addressed these questions by studying the functional consequences of the paired stimulation of cortical and thalamic projections in brain slices with a protocol resembling a temporal pattern of their activation *in vivo*. We found that the time-locked sequential activation of convergent auditory projections to the LAn induced ITDP[17] at the cortico-amygdala synapses.

RESULTS

Priming thalamic afferents induces ITDP in cortical input

We activated thalamic or cortical inputs to principal neurons in the LAn in brain slices, placing stimulation electrodes onto the internal capsule or the external capsule, respectively[12,15,18–23] (**Fig. 1** and **Supplementary Fig. 1a**,**b**; see Online Methods). Excitatory postsynaptic currents (EPSCs) were recorded under whole-cell voltage-clamp conditions at a holding potential of −70 mV in the presence of the GABA receptor A ($GABA_AR$) antagonist picrotoxin (50 μM). With our stimulation techniques, thalamic and cortical projections to the LAn were activated independently, as the arithmetic sum of the amplitudes of the EPSCs evoked by stimulation of either cortical or thalamic inputs separately was nearly identical to the EPSC amplitude when both inputs were stimulated simultaneously[15] (**Supplementary Fig. 1c**,**d**). Moreover, we did not observe cross-facilitation between the inputs, as stimulation of the cortical input with a single stimulus had no effect on the amplitude of the EPSC in the thalamic input evoked with a 50-ms delay, and vice versa (**Supplementary Fig. 1e**,**f**).

Previous *in vivo* recordings suggest that the signal from the auditory thalamus arrives to the LAn ~15–20 ms earlier than that from the auditory cortex[9,24,25]. This is because the auditory information that eventually enters the LAn from the cortex is first transmitted to the thalamus, then conveyed to the TE3 area of the auditory cortex, and is only then relayed to the LAn[21,25]. To investigate whether these two CSa pathways interact to affect synaptic responses in LAn principal

[1]Department of Psychiatry, McLean Hospital, Harvard Medical School, Belmont, Massachusetts, USA. [2]Department of Developmental Neurobiology, St. Jude Children's Research Hospital, Memphis, Tennessee, USA. Correspondence should be addressed to V.Y.B. (vadimb@mclean.harvard.edu).

Received 29 July; accepted 19 October; published online 11 December 2011; doi:10.1038/nn.2993

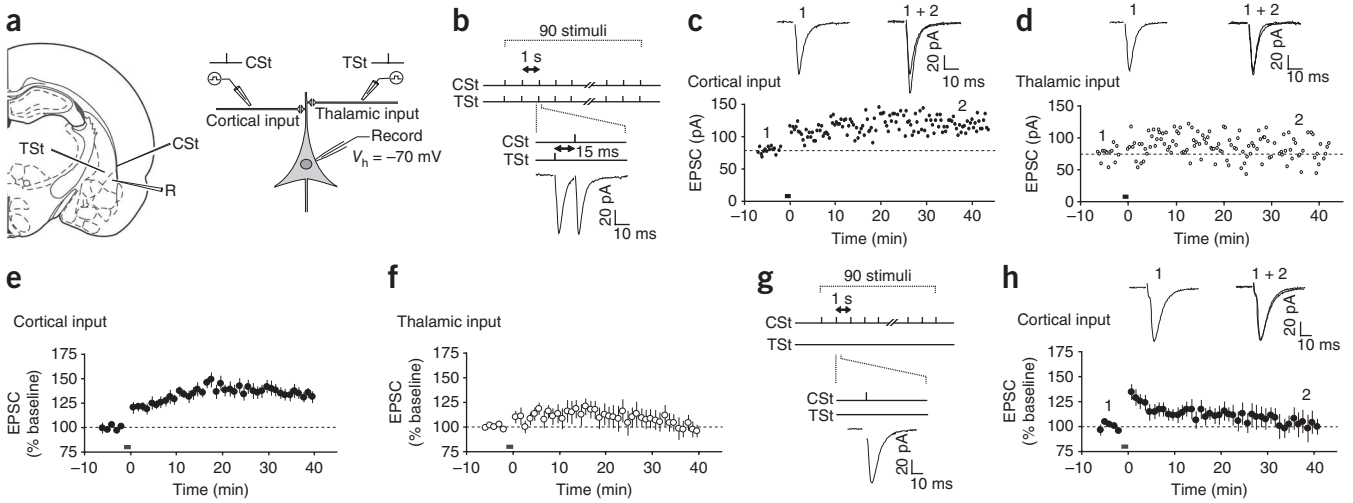

Figure 1 Paired stimulation of thalamic and cortical inputs induces ITDP at the cortico-LAn synapses. (**a**) Schematic representations of the slice preparation, showing positions of recording and stimulation electrodes (left), and the experimental design (right). Stimulation electrodes (CSt and TSt) were positioned to activate cortical or thalamic inputs, respectively. R, recording electrode. (**b**) A diagram illustrating the TSt-CSt protocol, consisting of paired stimulation of thalamic and cortical inputs. TSt was delivered 15 ms earlier than CSt. Below, examples of the EPSCs during the TSt-CSt stimulation. (**c**) TSt-CSt pairing–induced ITDP in cortical input to the LAn. Insets show the average of 15 cortico-LAn EPSCs recorded before (1) and 35–40 min after (2) the TCt-CSt stimulation (black horizontal bar). Stimulation artifacts were removed for clarity in these and all other examples of EPSCs. (**d**) EPSCs in thalamic input in the same experiment shown in **c**. Insets show the average of 15 thalamo-LAn EPSCs before (1) and after (2) the TSt-CSt stimulation. (**e**) Summary graph of all experiments shown in **c** ($n = 13$, paired t test, $P < 0.001$ versus baseline). The magnitude of potentiation was determined at 35–40 min after the induction. (**f**) Summary graph of all experiments shown in **d** ($n = 11$, $P = 0.53$ versus baseline). (**g**) Design of experiments in which TSt was omitted. (**h**) Potentiation of cortico-LAn EPSCs was not observed if only the cortical input was stimulated (black bar, $n = 6$, $P = 0.55$ versus baseline). Error bars indicate s.e.m.

neurons, we designed a stimulation protocol that approximately mimics the temporal relation of their activation in animals. It implicated continuous paired stimulation of the thalamic and cortical afferents with single presynaptic stimuli (TSt and CSt, respectively), delivered in such a manner that thalamic input was activated 15 ms before the stimulation of cortical input (TSt-CSt pairing protocol, $\Delta t = -15$ ms; **Fig. 1a**,**b**).

Paired stimulation of the thalamic and cortical inputs for 90 s at a 1-Hz frequency while the recorded postsynaptic neuron was voltage clamped at a holding potential of −70 mV resulted in substantial potentiation of the EPSC amplitude in the cortico-amygdala pathway (**Fig. 1c**,**e**). The amplitude of the EPSCs evoked by stimulation of the thalamic input, however, remained unaltered (**Fig. 1d**,**f**). The induction of potentiation in cortical input required priming stimulation of thalamic fibers, as stimulation of the cortical input alone at either 1-Hz (for 90 s) or 2-Hz (for 45 s) frequencies had no effect on the amplitude of cortico-LAn EPSCs (**Fig. 1g**,**h** and **Supplementary Fig. 2**). Under current-clamp recording conditions, when the postsynaptic membrane was allowed to depolarize during the induction, the TSt-CSt pairing protocol also induced potentiation of the excitatory postsynaptic potentials (EPSPs) in the cortical input to the LAn (**Supplementary Fig. 3a**,**b**). Temporal summation of the thalamic and cortical EPSPs, observed during the pairing of thalamic and cortical stimuli with a short interstimulus interval (15 ms), resulted in the averaged peak somatic depolarization of 10.1 ± 1.3 mV ($n = 6$), which did not lead to the spike firing in a recorded postsynaptic neuron (**Supplementary Fig. 3a**). Together, these findings indicate that the TSt-CSt pairing protocol induces ITDP[17] in the cortico-amygdala pathway.

Neurons in the LAn receive massive inhibitory inputs from the local circuit GABA-releasing interneurons[26–28], which control the susceptibility of synapses to LTP[22,29–31]. However, we found that the magnitude of ITDP in cortical input, induced in the absence of picrotoxin in the external medium (**Supplementary Fig. 3c**,**d**), was not different from that observed when inhibition was blocked (t test, $P = 0.11$; **Fig. 1e**). These results suggest that $GABA_A$R-mediated inhibition does not have a substantial effect on ITDP induction.

Time interval between TSt and CSt controls ITDP magnitude

We next examined whether the inducibility of ITDP depends on the time interval between activation of thalamic and cortical inputs during paired stimulation (**Fig. 2**). When the time interval between TSt and CSt was increased to 30 or 60 ms ($\Delta t = -30$ or -60 ms, respectively), the TSt-CSt pairing did not result in ITDP in cortical input (**Fig. 2a**,**d**,**e**). On the other hand, paired stimulation of thalamic and cortical inputs with $\Delta t = -8$ ms resulted in potentiation of the cortico-amygdala EPSC (**Fig. 2a** and **Supplementary Fig. 4a**). The magnitude of potentiation under these conditions was not significantly different from ITDP induced with $\Delta t = -15$ ms (t test, $P = 0.84$). The TSt-CSt stimulation with $\Delta t = -8$ ms also led to potentiation in the 'priming' pathway (thalamic input; **Fig. 2b** and **Supplementary Fig. 4a**), whereas the induction protocol with $\Delta t = -15$ ms resulted in ITDP in cortico-amygdala input only (**Fig. 2c**). Simultaneous activation of thalamic and cortical inputs ($\Delta t = 0$ ms) resulted in potentiation of both the cortico-amygdala and thalamo-amygdala EPSCs (**Fig. 2a**,**b** and **Supplementary Fig. 4b**). Thus, although ITDP in projections to the LAn could be induced at inter-input stimulation intervals shorter than 15 ms, the pathway specificity of ITDP was only maintained at the 15-ms delay between activation of thalamic and cortical fibers. These findings indicate that the inducibility and pathway-specificity of ITDP in the LAn is determined by the temporal delay between thalamic and cortical signals.

Reversing the temporal order of paired stimulation of cortical and thalamic pathways (the CSt-TSt protocol) was associated with the potentiation of thalamo-amygdala EPSCs ($\Delta t = +15$ ms; **Fig. 2b**,**f**),

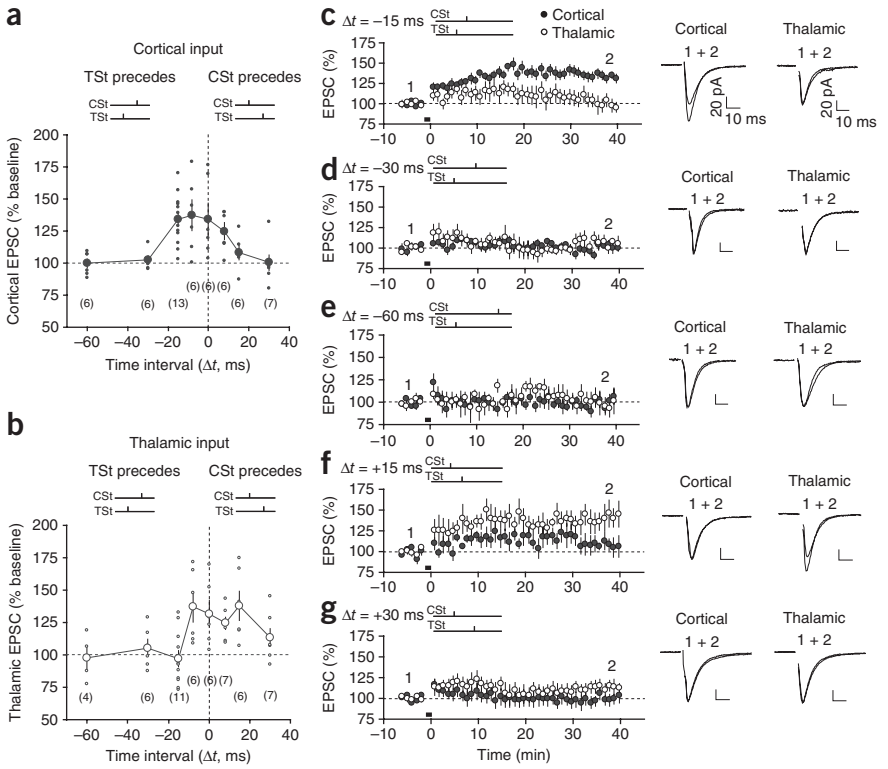

Figure 2 Dependence of ITDP induction on the time interval between TSt and CSt. (**a**) Normalized amplitude (% baseline) of the cortico-LAn EPSC at 35–40 min after paired stimulation when either the TSt preceded the CSt ($-\Delta t$) or the CSt preceded the TSt ($+\Delta t$). Time intervals during TSt-CSt paring (in ms): 0, –8, –15, –30 and –60; during CSt-TSt paring: +8, +15 and +30. Data points represent individual experiments. The number of experiments is indicated in parentheses. (**b**) Amplitude of the thalamo-LAn EPSC after paired stimulation (same experimental design as in **a**). (**c**) Summary graph demonstrating the time course of EPSC amplitude changes before and after TSt-CSt stimulation with $\Delta t = -15$ ms. Data shown in **Figure 1e**,**f** are included here for a comparison with other Δt. Traces are averages of 15 EPSCs recorded before (1) and after (2) the coactivation (black bar). (**d**) Data are presented as in **c**, but with $\Delta t = -30$ ms ($n = 6$, paired t test, $P = 0.50$ versus baseline in cortical input). (**e**) Data are presented as in **c** and **d**, but with $\Delta t = -60$ ms ($n = 6$, $P = 0.94$ versus baseline in cortical input). (**f**) Summary of experiments with $\Delta t = +15$ ms during the CSt-TSt paring ($n = 6$, $P < 0.05$ versus baseline in thalamic input, but $P = 0.27$ versus baseline in cortical input). (**g**) Data are presented as in **f**, but with $\Delta t = +30$ ms ($n = 7$). Scale bars represent 20 pA and 10 ms. Error bars indicate s.e.m.

whereas EPSCs in cortical projections did not exhibit significant enhancements (t test, $P = 0.27$ versus baseline). Following the delivery of the CSt-TSt stimulation with $\Delta t = +8$ ms, potentiation was observed in both thalamic and cortical inputs (**Fig. 2a**,**b** and **Supplementary Fig. 4c**). The CSt-TSt pairing with a longer interval ($\Delta t = +30$ ms) did not induce an increase of the EPSC amplitude in either thalamic or cortical inputs (**Fig. 2b**,**g**). These results suggest that both cortical and thalamic projections to the LAn possess the ability to undergo ITDP. However, ITDP in cortical input, induced by the TSt-CSt pairing, is likely to be more functionally relevant, as it may reflect the temporal order in which thalamic and cortical afferents are activated *in vivo*.

Glutamate uptake maintains pathway specificity of ITDP

Active glutamate uptake maintains input specificity of the conventional pairing-induced LTP in auditory inputs to the LAn, preventing heterosynaptic plasticity[15]. We explored the role of glutamate uptake in the induction of ITDP in the LAn, delivering the TSt-CSt paring stimulation protocol ($\Delta t = -15$ ms) at 22–25 °C. Glutamate transporters are highly temperature-sensitive and their functional efficiency is substantially diminished under such conditions[32]. In these experiments, the magnitude of ITDP was not different from that induced at more physiological temperatures (t test, $P = 0.58$; **Supplementary Fig. 5a**,**e**).

This potentiation, however, was no longer pathway specific, as the EPSC in thalamic input was also potentiated (**Supplementary Fig. 5b**,**e**). Moreover, following blockade of glutamate transporters with a specific inhibitor, DL-threo-β-benzyloxyaspartic acid (DL-TBOA, 10 μM), at physiological temperatures, the delivery of the TSt-CSt stimulation resulted in similar potentiation of the EPSC amplitude in cortical input (**Supplementary Fig. 5c**,**e**) and priming thalamic pathway ($P = 0.62$ for potentiation at cortical input versus potentiation at thalamic input, t test; **Supplementary Fig. 5d**,**e**). Thus, an efficient removal of released glutamate by glutamate transporters is required for maintaining pathway specificity of ITDP in the LAn.

Requirements for the induction of ITDP in the LAn

In the presence of the high-affinity Ca^{2+} chelator BAPTA (10 mM) in the recording pipette solution, the TSt-CSt pairing protocol (with a 15-ms interval) did not induce ITDP at the cortico-amygdala synapses (**Fig. 3a**,**b**), indicating that the rise in postsynaptic Ca^{2+} concentration is required for the induction process. Both NMDAR receptors (NMDARs) and L-type voltage-gated Ca^{2+} channels were previously identified as the sources of postsynaptic Ca^{2+} increases, triggering different forms of LTP in the LAn[12,15,22,33,34]. Notably, the induction of ITDP in the LAn did not depend on NMDAR activation, as it was not suppressed by the NMDAR antagonist D-2-amino-5-phosphonopentanoic acid (D-AP5, 50 μM; not significantly different from control ITDP, $P = 0.64$; **Fig. 3c**), whereas NMDAR EPSCs were completely blocked by the antagonist at this concentration (**Supplementary Fig. 6a**,**b**). The L-type Ca^{2+} blocker nitrendipine (20 μM) also had no effect on ITDP when applied alone (**Fig. 3d**) or jointly with D-AP5 (**Supplementary Fig. 7a–c**,**g**). We also re-tested the effects of D-AP5 on ITDP in the LAn by recoding synaptic responses in a current-clamp mode, thus allowing depolarization of the postsynaptic neuron during the TSt-CSt pairing. ITDP of the EPSPs in cortical input to the LAn was still not blocked in the presence of D-AP5 (**Supplementary Fig. 6c**,**d**; not significantly different from ITDP induced in the absence of D-AP5, $P = 0.49$; **Supplementary Fig. 3a**,**b**). These findings indicate that the postsynaptic Ca^{2+} influx, required for the induction of ITDP in the LAn, is not mediated by activation of NMDARs or L-type Ca^{2+} channels.

What are the cellular mechanisms implicated in the induction of ITDP in the LAn? Kainate glutamate receptors (KARs), specifically GluR5 (GluK1) subunit–containing receptor complexes, are highly expressed in the amygdala[35]. KARs have been shown to mediate the induction of a form of LTP in the basolateral amygdala[35], as well as LTP at the mossy fiber synapses in the hippocampus[36]. In our experiments, ITDP in cortical input was completely blocked in the presence of either UBP 296 (5 μM) or (*S*)-1-(2-amino-2-carboxyethyl)-3-(2-carboxy-5-phenylthiophene-3-yl-methyl)-5-methylpyrimidine-2,4-dione (ACET,

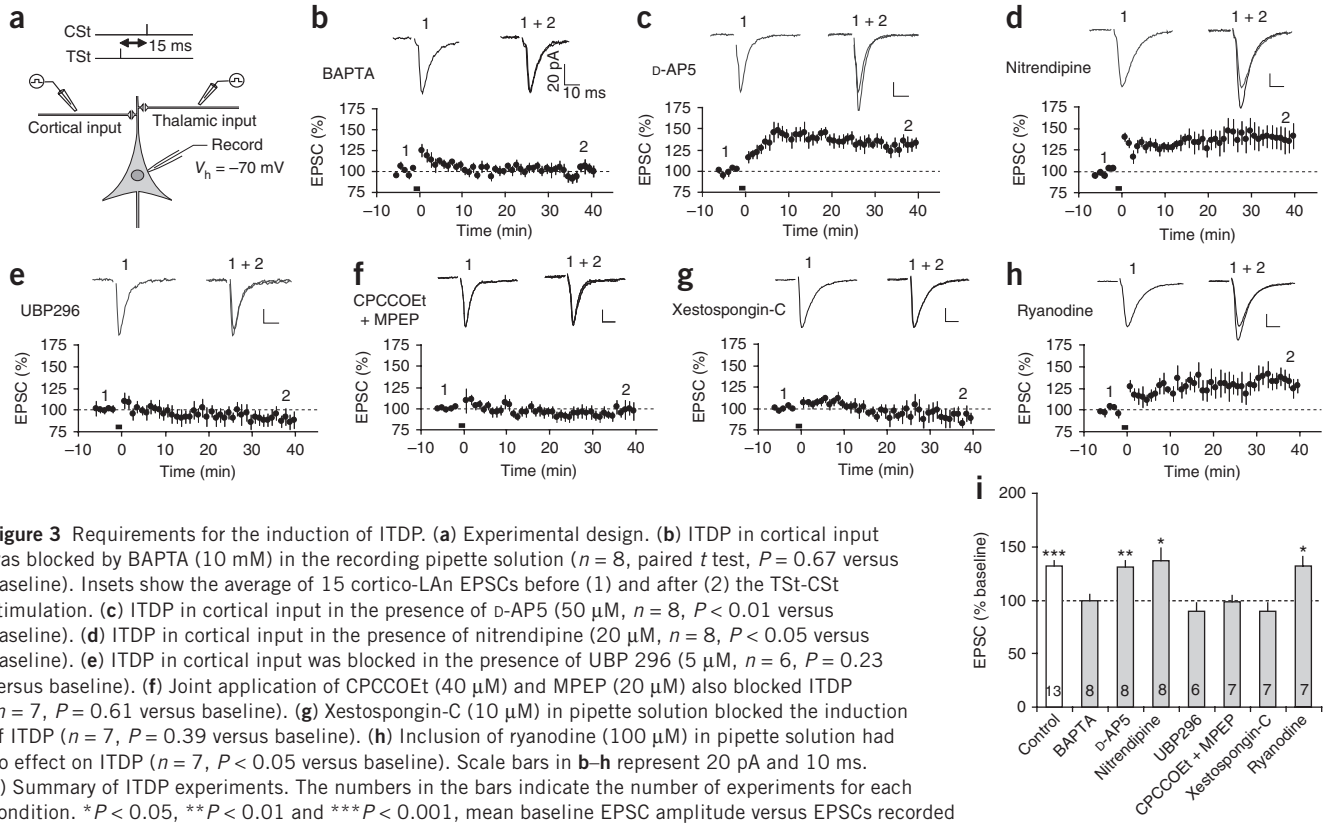

Figure 3 Requirements for the induction of ITDP. (**a**) Experimental design. (**b**) ITDP in cortical input was blocked by BAPTA (10 mM) in the recording pipette solution ($n = 8$, paired t test, $P = 0.67$ versus baseline). Insets show the average of 15 cortico-LAn EPSCs before (1) and after (2) the TSt-CSt stimulation. (**c**) ITDP in cortical input in the presence of D-AP5 (50 μM, $n = 8$, $P < 0.01$ versus baseline). (**d**) ITDP in cortical input in the presence of nitrendipine (20 μM, $n = 8$, $P < 0.05$ versus baseline). (**e**) ITDP in cortical input was blocked in the presence of UBP 296 (5 μM, $n = 6$, $P = 0.23$ versus baseline). (**f**) Joint application of CPCCOEt (40 μM) and MPEP (20 μM) also blocked ITDP ($n = 7$, $P = 0.61$ versus baseline). (**g**) Xestospongin-C (10 μM) in pipette solution blocked the induction of ITDP ($n = 7$, $P = 0.39$ versus baseline). (**h**) Inclusion of ryanodine (100 μM) in pipette solution had no effect on ITDP ($n = 7$, $P < 0.05$ versus baseline). Scale bars in **b**–**h** represent 20 pA and 10 ms. (**i**) Summary of ITDP experiments. The numbers in the bars indicate the number of experiments for each condition. $^*P < 0.05$, $^{**}P < 0.01$ and $^{***}P < 0.001$, mean baseline EPSC amplitude versus EPSCs recorded 35–40 min after the TSt-CSt pairing, paired t test. Error bars indicate s.e.m.

10 μM), specific antagonists of GluR5 KARs (**Fig. 3e** and **Supplementary Fig. 7d**,**g**), indicating that these receptors are involved in the induction process. GluR5 subunit–containing KARs were also implicated in the induction of heterosynaptic potentiation in thalamic input in the presence of DL-TBOA (10 μM) at physiological temperatures, as this potentiation was blocked by UBP 302 (**Supplementary Fig. 5f**).

Similar to hippocampal ITDP[17], ITDP in cortical input to the LAn was suppressed in the presence of the group I mGluR antagonists 7-(hydroxyimino)cyclopropa[*b*]chromen-1a-carboxylate ethyl ester (CPCCOEt, 40 μM) and 2-methyl-6-(phenylethynyl)pyridine hydrochloride (MPEP, 20 μM) (blocking mGluR1 and mGluR5 receptors, respectively; **Fig. 3f**) or LY 367385 (100 μM) and SIB 1757 (30 μM) (**Supplementary Fig. 7e**,**g**). The induction of ITDP was unaffected, however, by the antagonist of muscarinic acetylcholine receptors atropine (1 μM; **Supplementary Fig. 7f**,**g**). Release of Ca^{2+} from the internal stores is implicated, under certain conditions, in the induction of LTP[37,38] and, specifically, ITDP[17] at central synapses. Consistent with the role of Ca^{2+} release from the internal stores in ITDP induction, we found that ITDP in the amygdala was blocked when Xestospongin-C (10 μM), which inhibits $InsP_3$-sensitive Ca^{2+} stores, was included in pipette solution (**Fig. 3g**). However, ITDP was not affected by ryanodine (100 μM), blocking ryanodine receptor–mediated Ca^{2+} release (**Fig. 3h**,**i**).

The addition of a specific agonist of GluR5-containing KARs, (RS)-2-amino-3-(3-hydroxy-5-tert-butylisoxazol-4-yl)propanoic acid (ATPA, 1 μM), to the external solution did not result in potentiation of the cortico-amygdala EPSCs (**Fig. 4a**). The bath-applied agonist of group I mGluRs, (S)-3,5-dihydroxyphenylglycine ((S)-DHPG, 10 μM), also had no effect on the EPSC in cortical input (**Fig. 4b**). However, when applied together, ATPA and (S)-DHPG produced synaptic potentiation (**Fig. 4c**,**d**), indicating the need for a joint activation of both GluR5 KARs and group I mGluRs. Consistent with our finding that both cortical and thalamic projections to the LAn possess the ability to undergo ITDP, simultaneous application of ATPA and (S)-DHPG led to potentiation of the EPSC amplitude in the thalamic pathway (**Supplementary Fig. 8a**).

We also tested the possibility that the ATPA and (S)-DHPG–evoked potentiation of synaptic transmission in cortical input and ITDP, induced by electrical stimulation with the TSt-CSt pairing protocol, might occlude each other. In these experiments, we used the nystatin-based perforated patch-clamp technique, which minimizes the effects of postsynaptic 'washout' on the induction of synaptic plasticity. Under these conditions, the delivery of the TSt-CSt pairing protocol resulted in gradual potentiation of the EPSC amplitude, reaching the steady-state level by 20 min post-induction (**Fig. 4e**,**f**). Subsequent simultaneous application of ATPA (1 μM) and (S)-DHPG (10 μM) for 10 min did not lead to further increases in the EPSC amplitude (**Fig. 4e**,**f**), whereas their joint application without the preceding TSt-CSt pairing induced synaptic potentiation (**Fig. 4c**,**d**). Notably, agonist-induced synaptic potentiation without the prior induction of ITDP could be observed at later times during prolonged perforated patch-clamp recordings (**Supplementary Fig. 8b**,**c**). When the order of treatments was reversed, potentiation of the cortico-amygdala EPSC, induced by co-application of ATPA and DHPG for 10 min, occluded ITDP in response to the standard ITDP-inducing TSt-CSt stimulation (t test, $P = 0.55$; **Fig. 4g**,**h**). The mutual occlusion of the agonist-induced synaptic potentiation and ITDP indicates that they may be mechanistically similar, providing further support for the notion that activation of GluR5 KARs and group I mGluRs is required for the induction of ITDP in the LAn.

KARs mediate spatiotemporal summation of convergent inputs

We found that bath application of the GluR5 subunit–specific KAR agonist ATPA (0.1–10 μM) both with or without 10 mM BAPTA in

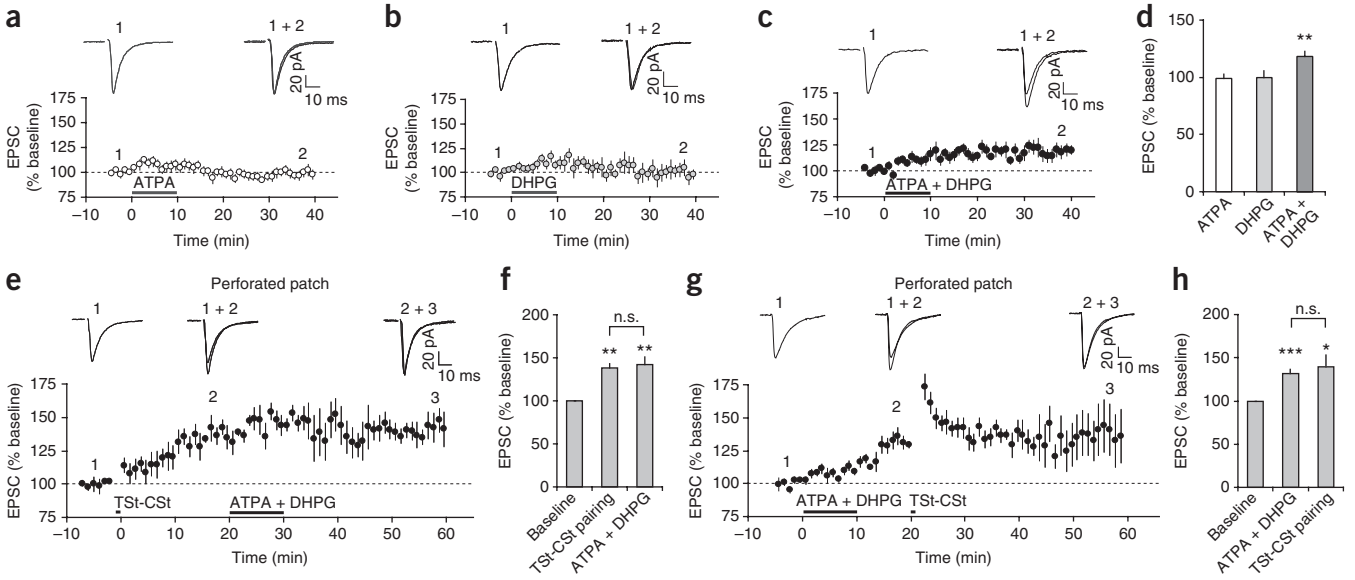

Figure 4 Coactivation of GluR5-containing KARs and group I mGluRs during ITDP induction. (**a**,**b**) Application of ATPA (1 μM) or (S)-DHPG (10 μM) alone did not potentiate the cortico-LAn EPSCs (ATPA, $n = 10$, $P = 0.76$ versus baseline; (S)-DHPG, $n = 6$, $P = 0.95$; paired t test). Insets show averaged cortico-LAn EPSCs recorded before (1) and at the end (2) of ATPA or (S)-DHPG application. (**c**) Applied jointly, ATPA and (S)-DHPG induced potentiation of the EPSC in cortical input ($n = 8$). (**d**) Summary of the ATPA and (S)-DHPG effects on cortico-LAn EPSCs (**$P < 0.01$ versus baseline). (**e**) Perforated patch technique was used in these experiments. The induction of ITDP (TSt-CSt pairing, $\Delta t = -15$ ms) occluded potentiation of the EPSC by jointly applied ATPA and (S)-DHPG ($n = 5$). (**f**) Summary of the experiments shown in **e**. Jointly applied ATPA and (S)-DHPG did not produce additional potentiation in cortical input ($n = 5$; n.s., $P = 0.49$ for ITDP magnitude versus potentiation with subsequently added agonists; paired t test). **$P < 0.01$ for both ITDP magnitude and potentiation after addition of agonists versus the baseline. (**g**) The order of treatments was reversed. Co-application of ATPA and (S)-DHPG preceded TSt-CSt stimulation ($n = 7$). (**h**) Summary of the experiments shown in **g**. ***$P < 0.001$ for agonist-induced potentiation and *$P < 0.05$ for the EPSC amplitude following TSt-CSt stimulation versus the baseline EPSC; n.s., no significant difference for agonist-induced potentiation versus ITDP magnitude, $P = 0.55$. Error bars indicate s.e.m.

pipette solution had no effect on the magnitude of paired-pulse facilitation (PPF), an index of presynaptic function[12] (**Supplementary Fig. 9**). This observation indicates that glutamate release is not directly regulated through activation of the GluR5 subunit–containing KARs on cortical terminals in the LAn. The joint application of ATPA and (S)-DHPG resulted in synaptic potentiation in the cortico-amygdala pathway (**Fig. 4c**,**d**), indicating that 1 μM ATPA is functionally active. Taken together, these results suggest that GluR5 KARs, which have been implicated in the induction of ITDP, do not directly control presynaptic function in the cortico-LAn projections and are likely to be expressed postsynaptically.

To evaluate a fractional contribution of postsynaptic KARs to the compound cortico-LAn and thalamo-LAn EPSCs, we recorded synaptic responses in the presence of D-AP5 (50 μM, $EPSC_{D\text{-}AP5}$) and then again after the addition of the AMPA receptor (AMPAR) antagonist SYM2206 (100 μM, $EPSC_{SYM2206}$)[39] to the external solution. It was followed by application of 2,3-dioxo-6-nitro-1,2,3,4-tetrahydrobenzo[*f*]quinoxaline-7-sulfonamide (NBQX, 10 μM, $EPSC_{NBQX}$), inhibiting both AMPARs and KARs (**Fig. 5a**). The KAR-mediated EPSC was isolated by subtracting $EPSC_{NBQX}$ from $EPSC_{SYM2206}$, whereas the AMPAR-mediated EPSC was isolated by subtracting $EPSC_{SYM2206}$ from $EPSC_{D\text{-}AP5}$. Using this approach, we found that 24 ± 2% ($n = 10$) and 22 ± 2% ($n = 9$) of the compound EPSC amplitude were mediated by KARs in cortical and thalamic inputs, respectively (no significant difference between inputs, $P = 0.87$ for AMPAR EPSC, $P = 0.64$ for KAR EPSC, t test; **Fig. 5b**). Consistent with these findings, bath application of the selective antagonist of GluR5 subunit–containing KARs UBP 302 (10 μM) resulted in a decrease of the EPSC amplitude in both cortical and thalamic inputs to 79 ± 3% ($n = 6$, $P < 0.001$) and 77 ± 1% ($n = 6$, $P < 0.001$) of the baseline value, respectively (**Supplementary Fig. 10a**,**b**). At this concentration, however, UBP 302 had no effect on PPF in either pathway (**Supplementary Fig. 10c**), suggesting that the reductions in the EPSC amplitude by UBP 302 were not a result of its presynaptic actions. Notably, a fractional contribution of the GluR5-KAR–mediated component was unchanged after the induction of ITDP (**Supplementary Fig. 10d**), indicating that different components of the postsynaptic response were increased proportionally at potentiated synapses. Consistent with previous findings[40], the decay time constant of KAR-mediated EPSCs in both inputs was greater than that of AMPAR EPSCs (**Fig. 5c**,**d**).

Given their slow decay kinetics, KAR-mediated EPSCs may display spatiotemporal summation during paired activation of thalamic and cortical afferents with short intervals. To address this possibility, we recorded isolated KAR-mediated EPSCs in the course of paired TSt-CSt stimulation, varying delays between cortical and thalamic stimuli. Indeed, we found that the amplitude of KAR EPSCs in cortical input was enhanced following priming of thalamic input. Spatiotemporal summation, resulting in the increased amplitude of the KAR EPSC in cortical input, was maximal at a 15-ms interval between the TSt and CSt (**Fig. 5e**,**f**). The EPSC in cortical input, however, displayed significantly reduced spatiotemporal summation when the delay between thalamic and cortical stimuli was 30 ms ($P < 0.05$ versus the 15-ms interval) or 60 ms ($P < 0.01$ versus the 15-ms interval). These results could, at least in part, explain the observation that the magnitude of ITDP reached its maximum level at a 15-ms time interval between activation of thalamic and cortical afferent fibers.

KARs at dendritic spines of LAn neurons are Ca^{2+} permeable

The finding that the induction of ITDP in the LAn was dependent on the rise in postsynaptic Ca^{2+} concentration, which was not mediated by NMDARs or L-type Ca^{2+} channels, whereas activation of

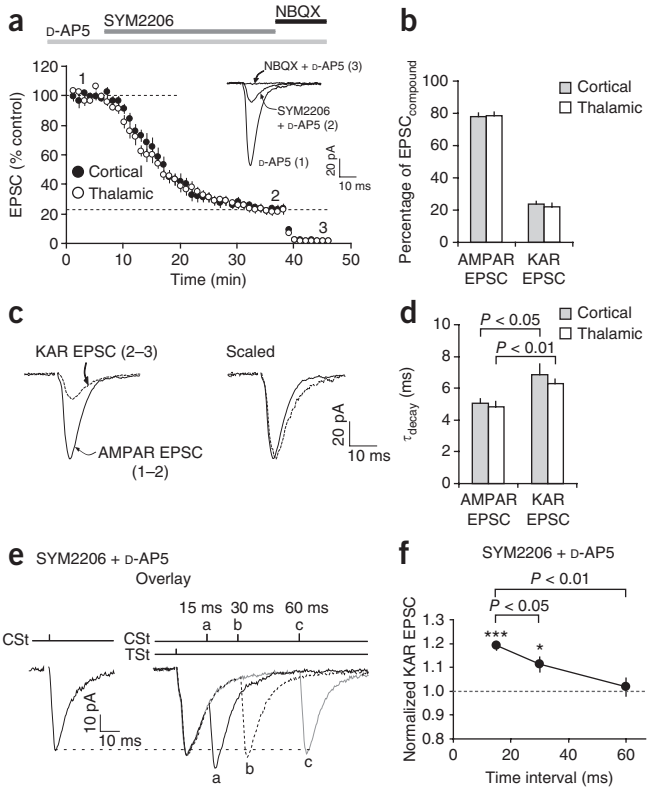

Figure 5 Spatiotemporal summation of KAR-mediated EPSCs during TSt-CSt stimulation. (**a**) Effects of SYM2206 (100 μM) and NBQX (10 μM) on the EPSC amplitude in cortical ($n = 10$) and thalamic ($n = 9$) inputs in the presence of D-AP5 (50 μM). Inset shows the averages of 15 traces under baseline conditions (1), during SYM2206-induced depression (2) and after NBQX addition (3). (**b**) Fractional contribution of the AMPAR- and KAR-mediated current components. To isolate the KAR-mediated EPSC, we subtracted $EPSC_{NBQX}$ (trace 3 in **a**) from $EPSC_{SYM2206}$ (trace 2). The AMPAR-mediated EPSC was isolated by subtracting $EPSC_{SYM2206}$ (trace 2) from $EPSC_{D\text{-}AP5}$ (trace 1). (**c**) Left, examples of isolated AMPAR- and KAR-mediated EPSCs. Right, same traces scaled by their peak amplitudes. (**d**) Decay time constants (from a single-exponential fit) of AMPAR EPSCs and KAR EPSCs in cortical ($n = 8$) and thalamic ($n = 8$) inputs. KAR-mediated EPSCs decayed significantly slower ($P < 0.05$ for cortical input, $P < 0.01$ for thalamic input, paired t test). (**e**) Left, KAR-mediated EPSC when cortical input was stimulated alone. Right, KAR-EPSCs when TSt preceded CSt by 15 ms (a), 30 ms (b), and 60 ms (c). (**f**) Spatiotemporal summation of KAR-mediated EPSCs depended on the time interval between TSt and CSt during paired stimulation. EPSCs were normalized to the EPSC evoked by CSt alone ($n = 7$, $^*P < 0.05$ for 30-ms delay and $^{***}P < 0.001$ for 15 ms-delay during the TSt-CSt pairing versus CSt alone, paired t test). Error bars indicate s.e.m.

GluR5-containing KARs was required to induce ITDP, suggests that KARs might provide an alternate route of postsynaptic Ca^{2+} delivery. It has been established previously that KARs composed of subunits from unedited mRNA at the glutamine/arginine site are Ca^{2+} permeable[41] and mediate inwardly rectifying currents when the intracellular solution contains polyamines[42,43]. We therefore examined the current-voltage (I-V) relationship of AMPAR and KAR EPSCs in cortical input to the LAn by recording evoked synaptic responses in a voltage-clamp mode over a range of membrane potentials from −70 to +50 mV. The I-V relation of AMPAR ESPCs (recorded in the presence of D-AP5, 50 μM) was linear, with a reversal potential −0.9 ± 0.6 mV ($n = 8$; **Fig. 6a**,**b**). In contrast, the I-V relation of KAR EPSCs (recorded in the presence of D-AP5 and SYM2206, 100 μM) exhibited partial inward rectification, as the amplitude of synaptic responses was diminished at +30 mV and +50 mV (**Fig. 6a**,**b**). The rectification index, defined as the EPSC amplitude at −50 mV divided by that at +50 mV ($EPSC_{-50mV}/EPSC_{+50mV}$), was significantly larger for

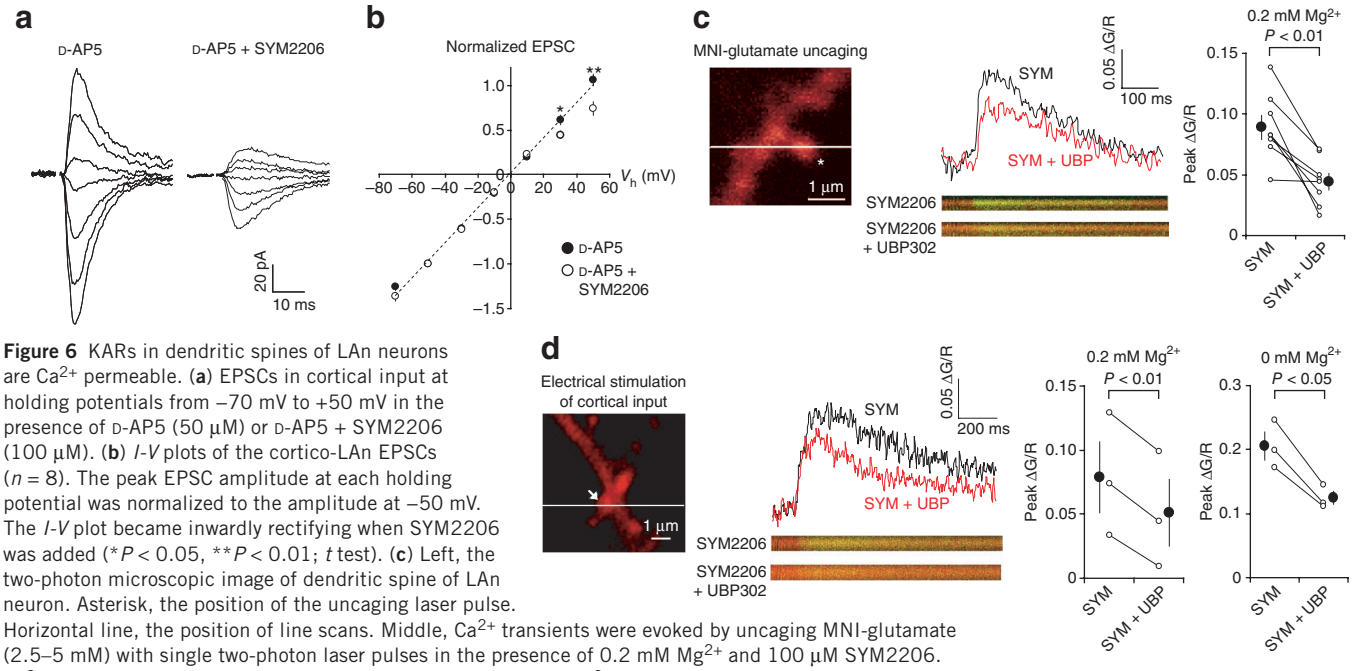

Figure 6 KARs in dendritic spines of LAn neurons are Ca^{2+} permeable. (**a**) EPSCs in cortical input at holding potentials from −70 mV to +50 mV in the presence of D-AP5 (50 μM) or D-AP5 + SYM2206 (100 μM). (**b**) I-V plots of the cortico-LAn EPSCs ($n = 8$). The peak EPSC amplitude at each holding potential was normalized to the amplitude at −50 mV. The I-V plot became inwardly rectifying when SYM2206 was added ($^*P < 0.05$, $^{**}P < 0.01$; t test). (**c**) Left, the two-photon microscopic image of dendritic spine of LAn neuron. Asterisk, the position of the uncaging laser pulse. Horizontal line, the position of line scans. Middle, Ca^{2+} transients were evoked by uncaging MNI-glutamate (2.5–5 mM) with single two-photon laser pulses in the presence of 0.2 mM Mg^{2+} and 100 μM SYM2206. Ca^{2+} transients were quantified as the ratio of change in green (Ca^{2+}-sensitive dye, Fluo-5F) to red (structural dye, Alexa 594) fluorescence (ΔG/R). The Ca^{2+} transient was reduced by UBP 302 (10 μM). Right, summary of the UBP 302 effects on Ca^{2+} transients (eight dendritic spines). (**d**) Left, dendritic spine (arrow) that was stimulated with electrical pulses delivered to cortical input in the presence of 0.2 mM Mg^{2+} and SYM2206. Middle, UBP 302 reduced synaptically induced Ca^{2+} transients in dendritic spine. Right, summary of UBP 302–induced changes in synaptically induced Ca^{2+} transients when external solution contained either 0.2 mM Mg^{2+} (three experiments) or 0 mM Mg^{2+} (three experiments). Error bars indicate s.e.m.

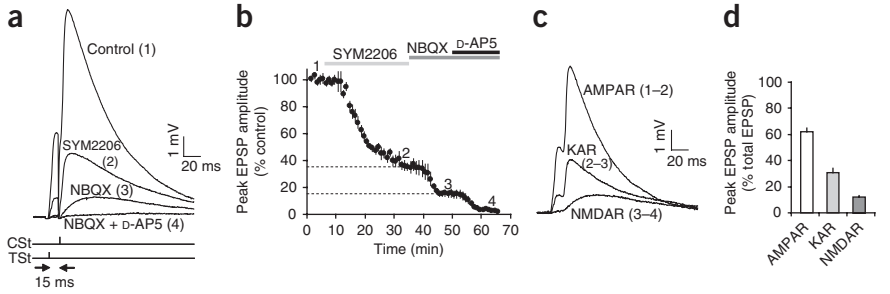

Figure 7 Fractional contribution of the AMPAR-, KAR- and NMDAR-mediated synaptic components to the compound EPSP during the TSt-CSt paired stimulation. (**a**) Examples of the EPSPs recorded in a LAn neuron in current-clamp mode evoked by paired stimulation of thalamic and cortical inputs with a 15-ms interval under control conditions (1) and in the presence of SYM2206 (2), NBQX (3) and NBQX + D-AP5 (4). Reponses were evoked once every 20 s. Note the spatiotemporal summation of EPSPs during the TSt-CSt paired stimulation. (**b**) Time course of the EPSP suppression during application of SYM2206, NBQX and NBQX + D-AP5 (indicated by bars above the graph). Peak amplitude of EPSPs was normalized to the baseline EPSP amplitude ($n = 6$). (**c**) Examples of isolated (subtracted) AMPAR-, KAR- and NMDAR-mediated EPSPs from an experiment shown in **a**: $EPSP_{AMPAR} = EPSP_{control} - EPSP_{SYM2206}$; $EPSP_{KAR} = EPSP_{SYM2206} - EPSP_{NBQX}$; $EPSP_{NMDAR} = EPSP_{NBQX} - EPSP_{NBQX + D\text{-}AP5}$. (**d**) Fractional contribution of the AMPAR-, KAR- and NMDAR-mediated EPSPs in the compound EPSP (based on the peak amplitude measurements) during paired TSt-CSt stimulation ($n = 6$). Error bars indicate s.e.m.

KAR-mediated EPSCs than for AMPAR-mediated EPSCs (1.44 ± 0.20 for KAR EPSCs; 0.97 ± 0.05 for AMPAR EPSCs; *t* test, $P < 0.05$). These findings suggest that at least a fraction of KARs activated by stimulation of cortical input might be Ca^{2+} permeable.

We directly tested whether synaptically activated KARs could mediate Ca^{2+} influx at dendritic spines of LAn neurons by visualizing calcium transients in spines with two-photon imaging. We induced Ca^{2+} transients using either two-photon photolysis (uncaging) of 4-methoxy-7-nitroindolinyl-caged-L-glutamate (MNI-glutamate) or synaptic stimulation. Using whole-cell patch pipettes, we loaded principal neurons with the cytoplasmic dye Alexa 594 (60 μM) and the Ca^{2+} indicator Fluo-5F (300 μM). The slices were perfused with the external solution containing a low Mg^{2+} (0.2 mM), MNI-glutamate (2.5–5 mM) and SYM2206 (100 μM). Glutamate uncaging with the single two-photon laser pulses induced Ca^{2+} transients in the dendritic spine (**Fig. 6c**). The peak amplitudes of Ca^{2+} transients, induced by uncaged glutamate, were significantly reduced by UBP 302, a selective antagonist of GluR5 subunit–containing KARs (10 μM, $n = 8$ spines, $P < 0.01$, *t* test; **Fig. 6c**). This indicates that the recorded Ca^{2+} transients were partly mediated by activation of KARs. The residual Ca^{2+} transients recorded in the presence of SYM2206 and UBP 302 were blocked by D-AP5 (50 μM) and were therefore mediated by NMDARs (**Supplementary Fig. 11a**,**b**).

In a different set of experiments, we searched for dendritic spines that responded to electrical stimulation of cortical inputs to the LAn. Synaptically induced Ca^{2+} transients were significantly reduced when UBP 302 (10 μM) was added to the external solution ($n = 3$ spines, $P < 0.01$, *t* test; **Fig. 6d**). However, activation of KARs by uncaged or synaptically released glutamate, leading to postsynaptic depolarization, could further relieve the voltage-dependent Mg^{2+} block, possibly resulting in a component of the spine Ca^{2+} influx through NMDAR channels, which would be sensitive to the KAR antagonist. We therefore tested the effect of UBP 302 on spine Ca^{2+} transients without added Mg^{2+} in the external medium when the Mg^{2+} block of NMDAR channels is fully relieved. Under these recording conditions, spine Ca^{2+} transients, induced by stimulation of cortical input in the presence of the AMPAR antagonist SYM2206 (100 μM), were still significantly reduced by UBP 302 (10 μM) ($n = 3$ spines, $P < 0.05$, paired *t* test; **Fig. 6d**). Notably, UBP 302 in this concentration had no direct effect on the amplitude of isolated NMDAR-mediated cortico-LAn EPSCs (**Supplementary Fig. 11c**,**d**). Taken together, these findings provide evidence that GluR5 subunit–containing KARs in dendritic spines of LAn neurons are Ca^{2+} permeable.

Testing the role of these receptors in the induction process, we found that ITDP was blocked when the TSt-CSt paired stimulation was delivered in the presence of 1-naphthyl acetyl spermine (NASPM, 100 μM), a synthetic analog of Joro spider toxin (**Supplementary Fig. 12c**) that is known to block Ca^{2+}-permeable AMPARs and KARs[44]. At this concentration, NASPM caused significant reductions (paired *t* test, $P < 0.01$ versus baseline) in the amplitude of isolated KAR EPSCs (recorded in the presence of 100 μM SYM2206), whereas AMPAR EPSCs (recorded in the presence of 10 μM UBP 302) were unaffected (**Supplementary Fig. 12a**,**b**). These results support the notion that Ca^{2+}-permeable KARs are required for the induction of ITDP in the LAn.

Synaptically evoked Ca^{2+} transients in dendritic spines were only partially blocked by the KAR antagonist, whereas a fraction of the Ca^{2+} signal was mediated by activation of NMDARs (**Fig. 6d** and **Supplementary Fig. 11a**,**b**). However, the induction of ITDP in cortical input did not depend on NMDARs (**Fig. 3c**,**i** and **Supplementary Fig. 6c**,**d**). To further characterize the conditions underlying ITDP induction, we estimated the magnitudes of the KAR-mediated and NMDAR-mediated EPSPs during delivery of the TSt-CSt stimulation protocol in the current-clamp recording mode in the presence of the physiological concentration of external Mg^{2+} (1 mM, same concentration of Mg^{2+} as was used in the induction of ITDP). EPSPs were evoked by the paired stimulation of thalamic and cortical inputs with a 15-ms interval. Stimulation of cortical input, following activation of the thalamic pathway, resulted in a prominent summation of thalamic and cortical synaptic responses (**Fig. 7a**). We quantified fractional contributions of the KAR- and NMDAR-mediated components of synaptic responses into the compound EPSP by subtracting traces recorded in the presence of SYM2206 (100 μM), NBQX (10 μM; **Fig. 7a**,**b**), which also blocks KARs, and D-AP5 (50 μM; **Fig. 7a**,**b**) from baseline responses and from each other (**Fig. 7c**). We found that nearly 30% of the EPSP, evoked by the TSt-CSt paired stimulation, was mediated by activation of KARs (**Fig. 7d**), whereas the contribution of the NMDAR-mediated EPSP was small (~10% of a total EPSP amplitude at the resting membrane potential). Similar estimates were obtained in the experiments where the effect of D-AP5 (50 μM) on the EPSP amplitude was tested first (before blocking the AMPAR and KAR component; **Supplementary Fig. 13**). Evidently, postsynaptic depolarization during the TSt-CSt pairing was insufficient to fully relieve the Mg^{2+} block of NMDARs, whereas KARs (which do not require postsynaptic depolarization for their activation) were fully functional under such conditions and could provide the Ca^{2+} required for the induction of ITDP.

Contribution of ITDP-like mechanisms in fear conditioning

If ITDP, which is sensitive to the blockade of GluR5 subunit–containing KARs, is involved in fear conditioning, then inhibition

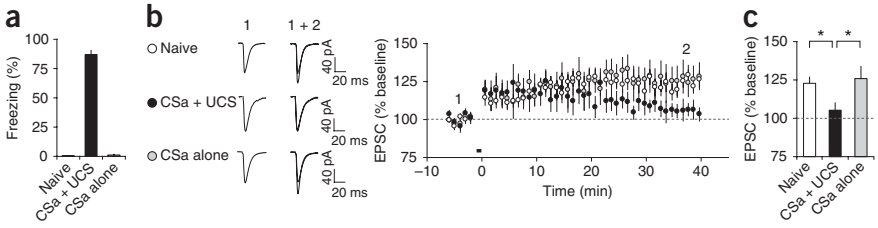

Figure 8 ITDP in cortico-LAn pathway is occluded in slices from fear-conditioned rats. (**a**) Freezing responses following single-trial auditory fear conditioning (CSa + UCS group) and freezing in behaviorally naive rats and rats that received the CSa only. (**b**) Left, representative cortico-LAn EPSCs (averages of ten responses) recorded before (1) and after (2) the delivery of the TSt-CSt protocol ($\Delta t = -15$ ms) in slices from all experimental groups (naive, CSa + UCS, and CSa alone). Right, ITDP at the cortico-LAn synapses was occluded in slices from fear-conditioned rats ($n = 12$ neurons from 8 rats, paired t test, $P = 0.18$ versus the baseline amplitude), whereas significant ITDP was observed in behaviorally naive rats ($n = 14$ neurons from 9 rats, $P < 0.001$ versus baseline) or the CSa alone rats ($n = 7$ neurons from 4 rats, $P < 0.05$ versus baseline). (**c**) Summary of the EPSC amplitude changes in cortical input following the TSt-CSt paired stimulation (as in **b**) in slices from different experimental groups of rats. $^*P < 0.05$, CSa + UCS group versus naive or CSa alone group, one-way ANOVA with *post hoc* Bonferroni simultaneous tests. Error bars are s.e.m.

of KARs should interfere with the acquisition of conditioned fear memory. Consistent with this prediction, we found that pre training bilateral intra-amygdala microinfusions of the specific GuR5 subunit–containing KAR antagonist UBP 302 suppressed fear learning. UBP 302–injected rats froze significantly less at 48 h post-training in response to the conditioned tone compared with vehicle-injected rats ($P < 0.01$ between groups; **Supplementary Fig. 14**), confirming the role of KAR-dependent processes in the amygdala, such as ITDP, in auditory fear conditioning.

To explore further the role of ITDP in fear conditioning, we tested ITDP in slices from conditioned rats. Memory of fear was assessed by measuring an increase in the freezing response to the tone following fear conditioning (**Fig. 8a**). Shortly after the fear memory test, we performed whole-cell recordings from neurons in slices from conditioned or control rats. We found that virtually no potentiation could be observed in cortical input to the LAn in slices from conditioned rats (CSa-UCS group) at 35–40 min after the delivery of the TSt-CSt pairing induction protocol ($\Delta t = -15$ ms, t test, $P = 0.18$ versus baseline; **Fig. 8b**,**c**). However, normal ITDP was observed in slices from behaviorally naive rats ($P < 0.001$ versus baseline) or rats that received just the CSa ($P < 0.05$ versus baseline). These findings indicate that ITDP in cortical input to the LAn is occluded following the acquisition of fear memory to the CSa, suggesting that ITDP-like mechanisms may contribute to encoding the fear memory trace.

Using the nystatin-based perforated patch-clamp technique, we also found that the NMDAR-dependent form of LTP, which was induced by pairing presynaptic stimulation at a 2-Hz frequency and postsynaptic depolarization to +30 mV[12], did not occlude the induction of ITDP (**Supplementary Fig. 15**). Thus, these two forms of synaptic plasticity at the LAn synapses may contribute to the encoding of conditioned fear memory, synergistically increasing the magnitude of synaptic responses in the CSa pathways during the conditioned stimulus presentation.

DISCUSSION

Our results indicate that continuous low-frequency paired activation of thalamic and cortical auditory inputs with the 15-ms timing delay induces persistent synaptic potentiation at the cortico-amygdala synapses. This induction protocol approximately resembles a temporal pattern of synaptic activation *in vivo*, as a direct thalamic input may deliver the acoustic signals to the LAn ~15–20 ms earlier than an indirect thalamo-cortico-LAn projection[9,24]. The observed form of ITDP, resulting from associative interactions between two CSa pathways in the LAn, is different from a previously described form of heterosynaptic plasticity that could be triggered in cortical input by subthreshold stimulation of cortical and thalamic afferents with short trains of presynaptic pulses at much higher frequencies (30 Hz) and is induced entirely presynaptically[45]. ITDP is a newly discovered form of synaptic plasticity that was originally observed in the hippocampus, where pairing of subthreshold stimulation of the distal perforant path-CA1 synapses and the proximal Schaffer collateral-CA1 synapses resulted in potentiation of the Schaffer collateral EPSP when the inputs were activated at a precise interval[17].

ITDP in the cortico-LAn projections, explored by us, is mechanistically distinct from a slowly developing form of heterosynaptic potentiation in inputs to LAn neurons that could be induced by prolonged low-frequency stimulation of cortical fibers alone[35]. ITDP in cortical input to the LAn, which required joint activation of cortical and thalamic afferents for its induction, was pathway specific at physiological temperatures (not heterosynaptic), suggesting a potential functional role for this newly discovered form of synaptic plasticity in the CSa pathways at the behavioral level. Consistent with this notion, ITDP was occluded in slices from fear-conditioned rats. Moreover, similar to ITDP, the acquisition of fear memory was sensitive to the blockade of the GluR5-containing KARs (but see ref. 40). These findings indicate that ITDP-like synaptic enhancements in cortical input to the LAn might be recruited during fear conditioning.

Insufficient postsynaptic depolarization during the induction process could explain why ITDP in the LAn, while implicating an increase in the postsynaptic Ca^{2+} concentration, does not depend on the activation of NMDARs (unlike ITDP in the hippocampus that is NMDAR dependent[17]) or L-type voltage-gated calcium channels. Ca^{2+} release from the $InsP_3$-sensitive internal stores, which is possibly mediated by synaptic activation of group I mGluRs, contributes to the rises in a postsynaptic Ca^{2+} concentration in LAn neurons during the ITDP-inducing stimulation. Notably, the acquisition of conditioned fear memory was shown to depend on the activation of group I mGluRs in the amygdala[46]. As we found using two-photon imaging and glutamate uncaging, GluR5 subunit–containing KARs in the LAn are Ca^{2+} permeable, and therefore provide a likely route for postsynaptic Ca^{2+} delivery during ITDP induction. Consistent with this notion, approximately 30% of GluR5 mRNA in the amygdala is present in an unedited form[35]. KARs that are composed of subunits unedited in their glutamine/arginine site display Ca^{2+} permeability, whereas KARs containing subunits from edited mRNA are Ca^{2+} impermeable[41]. ITDP was prevented when either of the inductive calcium signals, the release of Ca^{2+} from the internal stores as a result of activation of group I mGluRs or postsynaptic Ca^{2+} influx through calcium-permeable KARs, was suppressed. This could indicate that the threshold intracellular Ca^{2+} concentration, which is required for the induction of ITDP in the LAn, could only be reached when both sources of postsynaptic calcium are simultaneously recruited during the induction process. As the mGluR-mediated Ca^{2+} release is not time locked, the temporal requirements for the

induction of ITDP are likely to be mediated by the characteristics of GluR5-KAR–mediated synaptic responses in convergent projections to the LAn. Spatiotemporal summation of the slowly decaying KAR-mediated EPSCs during paired activation of the thalamic and cortical afferents resulted in the enlargement of the KAR-mediated synaptic responses in cortical input, which was most prominent when the interval between thalamic and cortical signals converging in the LAn was matched to the ~15-ms delay. This finding implies that the cellular machinery involved in the induction of ITDP in the LAn and in maintaining its pathway specificity might be finely tuned to detect temporal patterns of activation in the CSa pathways.

Recent combined electrophysiological and imaging studies provide evidence that cortical and thalamic afferents could converge on the same dendritic branch, forming active synapses on spines, which could be as close as <5 μm[47]. Nevertheless, thalamic and cortical inputs function independently under the conditions of the low-frequency basal presynaptic activity. The pathway specificity of ITDP at the LAn synapses is controlled by active glutamate uptake and is only lost when glutamate transporters are inactivated. Thus, it is unlikely that the diffusion of glutamate from thalamic to cortical input would contribute to the induction of ITDP. Given that ITDP in the LAn requires an increase in postsynaptic Ca^{2+} concentration, the interaction between synapses activated by thalamic and cortical fibers is likely to occur in the dendritic branch. A recent study found that the induction of LTP at an individual synapse could be associated with the reduction of the threshold for LTP induction at neighboring dendritic spines[48]. By analogy, during the induction of ITDP in the LAn, the instructive signal resulting from the priming activation of thalamic input could spread from thalamic spines to the closely located spines possessing synapses activated by cortical fibers, thus facilitating the induction of ITDP in cortical pathway.

Although the temporal patterns of the signals' flow in the CSa projections during behavioral training might be more complex than that modeled here, our results nevertheless provide evidence that ITDP might be functionally relevant. The firing rates of neurons in the LAn are notoriously low both under baseline conditions and during the acquisition of fear memory[49]. The levels of presynaptic activity associated with the CSa presentation might be insufficient to produce the functionally relevant membrane depolarization in LAn neurons during behavioral training. ITDP, possibly acting in concert with the conventional NMDAR-dependent forms of synaptic plasticity (which result from the CSa-UCS pairing and also contribute to the acquisition of fear memory[12,34]), could provide an additional mechanism of synaptic strengthening in the CSa pathways that is nearly entirely determined by the spatiotemporal characteristics of the convergent presynaptic activity patterns.

METHODS

Methods and any associated references are available in the online version of the paper at http://www.nature.com/natureneuroscience/.

Note: Supplementary information is available on the Nature Neuroscience website.

ACKNOWLEDGMENTS

We thank Y. Li and K. Tully for constructive discussions. This study was supported by US National Institutes of Health grants MH083011, MH090464 (V.Y.B.) and MH079079 (S.S.Z.), the National Alliance for Research on Schizophrenia and Depression (V.Y.B.), Whitehall Foundation (V.Y.B.), and US Army Medical Research Acquisition Activity grant #W81XWH-08-2-0126 (V.Y.B.).

AUTHOR CONTRIBUTIONS

J.-H.C., I.T.B., E.G.M., K.M.M., W.A.C. and S.S.Z. performed the experiments and analyzed the results. V.Y.B. and J.-H.C. designed the experiments, interpreted the results and wrote the paper.

COMPETING FINANCIAL INTERESTS

The authors declare no competing financial interests.

Published online at http://www.nature.com/natureneuroscience/.
Reprints and permissions information is available online at http://www.nature.com/reprints/index.html.

1. LeDoux, J.E. Emotion circuits in the brain. *Annu. Rev. Neurosci.* **23**, 155–184 (2000).
2. Maren, S. & Quirk, G.J. Neuronal signalling of fear memory. *Nat. Rev. Neurosci.* **5**, 844–852 (2004).
3. Romanski, L.M. & LeDoux, J.E. Equipotentiality of thalamo-amygdala and thalamo-cortico-amygdala circuits in auditory fear conditioning. *J. Neurosci.* **12**, 4501–4509 (1992).
4. Campeau, S. & Davis, M. Involvement of subcortical and cortical afferents to the lateral nucleus of the amygdala in fear conditioning measured with fear-potentiated startle in rats trained concurrently with auditory and visual conditioned stimuli. *J. Neurosci.* **15**, 2312–2327 (1995).
5. Armony, J.L., Servan-Schreiber, D., Romanski, L.M., Cohen, J.D. & LeDoux, J.E. Stimulus generalization of fear responses: effects of auditory cortex lesions in a computational model and in rats. *Cereb. Cortex* **7**, 157–165 (1997).
6. Clugnet, M.C. & LeDoux, J.E. Synaptic plasticity in fear conditioning circuits: induction of LTP in the lateral nucleus of the amygdala by stimulation of the medial geniculate body. *J. Neurosci.* **10**, 2818–2824 (1990).
7. Bordi, F. & LeDoux, J.E. Response properties of single units in areas of rat auditory thalamus that project to the amygdala. II. Cells receiving convergent auditory and somatosensory inputs and cells antidromically activated by amygdala stimulation. *Exp. Brain Res.* **98**, 275–286 (1994).
8. Quirk, G.J., Repa, C. & LeDoux, J.E. Fear conditioning enhances short-latency auditory responses of lateral amygdala neurons: parallel recordings in the freely behaving rat. *Neuron* **15**, 1029–1039 (1995).
9. Quirk, G.J., Armony, J.L. & LeDoux, J.E. Fear conditioning enhances different temporal components of tone-evoked spike trains in auditory cortex and lateral amygdala. *Neuron* **19**, 613–624 (1997).
10. Rogan, M.T., Staubli, U.V. & LeDoux, J.E. Fear conditioning induces associative long-term potentiation in the amygdala. *Nature* **390**, 604–607 (1997).
11. McKernan, M.G. & Shinnick-Gallagher, P. Fear conditioning induces a lasting potentiation of synaptic currents *in vitro*. *Nature* **390**, 607–611 (1997).
12. Tsvetkov, E., Carlezon, W.A., Benes, F.M., Kandel, E.R. & Bolshakov, V.Y. Fear conditioning occludes LTP-induced presynaptic enhancement of synaptic transmission in the cortical pathway to the lateral amygdala. *Neuron* **34**, 289–300 (2002).
13. Rumpel, S., LeDoux, J., Zador, A. & Malinow, R. Postsynaptic receptor trafficking underlying a form of associative learning. *Science* **308**, 83–88 (2005).
14. Shumyatsky, G.P. *et al. Stathmin*, a gene enriched in the amygdala, controls both learned and innate fear. *Cell* **123**, 697–709 (2005).
15. Tsvetkov, E., Shin, R.M. & Bolshakov, V.Y. Glutamate uptake determines pathway specificity of long-term potentiation in the neural circuitry of fear conditioning. *Neuron* **41**, 139–151 (2004).
16. Doyère, V., Schafe, G.E., Sigurdsson, T. & LeDoux, J.E. Long-term potentiation in freely moving rats reveals asymmetries in thalamic and cortical inputs to the lateral amygdala. *Eur. J. Neurosci.* **17**, 2703–2715 (2003).
17. Dudman, J.T., Tsay, D. & Siegelbaum, S.A. A role for synaptic inputs at distal dendrites: instructive signals for hippocampal long-term plasticity. *Neuron* **56**, 866–879 (2007).
18. Mahanty, N.K. & Sah, P. Calcium-permeable AMPA receptors mediate long-term potentiation in interneurons in the amygdala. *Nature* **394**, 683–687 (1998).
19. LeDoux, J.E., Ruggiero, D.A. & Reis, D.J. Projections to the subcortical forebrain from anatomically defined regions of the medial geniculate body in the rat. *J. Comp. Neurol.* **242**, 182–213 (1985).
20. Mascagni, F., McDonald, A.J. & Coleman, J.R. Corticoamygdaloid and corticocortical projections of the rat temporal cortex: a *Phaseolus vulgaris* leucoagglutinin study. *Neuroscience* **57**, 697–715 (1993).
21. Romanski, L.M. & LeDoux, J.E. Information cascade from primary auditory cortex to the amygdala: corticocortical and corticoamygdaloid projections of temporal cortex in the rat. *Cereb. Cortex* **3**, 515–532 (1993).
22. Shin, R.M., Tsvetkov, E. & Bolshakov, V.Y. Spatiotemporal asymmetry of associative synaptic plasticity in fear conditioning pathways. *Neuron* **52**, 883–896 (2006).
23. Shin, R.M. *et al.* Hierarchical order of coexisting pre- and postsynaptic forms of long-term potentiation at synapses in amygdala. *Proc. Natl. Acad. Sci. USA* **107**, 19073–19078 (2010).
24. Li, X.F., Stutzmann, G.E. & LeDoux, J.E. Convergent but temporally separated inputs to lateral amygdala neurons from the auditory thalamus and auditory cortex use different postsynaptic receptors: *in vivo* intracellular and extracellular recordings in fear conditioning pathways. *Learn. Mem.* **3**, 229–242 (1996).
25. Johnson, L.R. *et al.* A recurrent network in the lateral amygdala: a mechanism for coincidence detection. *Front. Neural Circuits* **2**, 3 (2008).
26. Sugita, S., Tanaka, E. & North, R.A. Membrane properties and synaptic potentials of three types of neurone in rat lateral amygdala. *J. Physiol. (Lond.)* **460**, 705–718 (1993).

27. Li, X.F., Armony, J.L. & LeDoux, J.E. GABAA and GABAB receptors differentially regulate synaptic transmission in the auditory thalamo-amygdala pathway: an *in vivo* microiontophoretic study and a model. *Synapse* **24**, 115–124 (1996).
28. Lang, E.J. & Paré, D. Similar inhibitory processes dominate the responses of cat lateral amygdaloid projection neurons to their various afferents. *J. Neurophysiol.* **77**, 341–352 (1997).
29. Bissière, S., Humeau, Y. & Lüthi, A. Dopamine gates LTP induction in lateral amygdala by suppressing feedforward inhibition. *Nat. Neurosci.* **6**, 587–592 (2003).
30. Kodirov, S.A. *et al.* Synaptically released zinc gates long-term potentiation in fear conditioning pathways. *Proc. Natl. Acad. Sci. USA* **103**, 15218–15223 (2006).
31. Tully, K., Li, Y., Tsvetkov, E. & Bolshakov, V.Y. Norepinephrine enables the induction of associative long-term potentiation at thalamo-amygdala synapses. *Proc. Natl. Acad. Sci. USA* **104**, 14146–14150 (2007).
32. Asztely, F., Erdemli, G. & Kullmann, D.M. Extrasynaptic glutamate spillover in the hippocampus: dependence on temperature and the role of active glutamate uptake. *Neuron* **18**, 281–293 (1997).
33. Huang, Y.Y. & Kandel, E.R. Postsynaptic induction and PKA-dependent expression of LTP in the lateral amygdala. *Neuron* **21**, 169–178 (1998).
34. Bauer, E.P., Schafe, G.E. & LeDoux, J.E. NMDA receptors and L-type voltage-gated calcium channels contribute to long-term potentiation and different components of fear memory formation in the lateral amygdala. *J. Neurosci.* **22**, 5239–5249 (2002).
35. Li, H., Chen, A., Xing, G., Wei, M.L. & Rogawski, M.A. Kainate receptor–mediated heterosynaptic facilitation in the amygdala. *Nat. Neurosci.* **4**, 612–620 (2001).
36. Bortolotto, Z.A. *et al.* Kainate receptors are involved in synaptic plasticity. *Nature* **402**, 297–301 (1999).
37. Raymond, C.R. & Redman, S.J. Different calcium sources are narrowly tuned to the induction of different forms of LTP. *J. Neurophysiol.* **88**, 249–255 (2002).
38. Bardo, S., Cavazzini, M.G. & Emptage, N. The role of the endoplasmic reticulum Ca^{2+} store in the plasticity of central neurons. *Trends Pharmacol. Sci.* **27**, 78–84 (2006).
39. Li, P. *et al.* Kainate-receptor–mediated sensory synaptic transmission in mammalian spinal cord. *Nature* **397**, 161–164 (1999).
40. Ko, S., Zhao, M.G., Toyoda, H., Qiu, C.S. & Zhuo, M. Altered behavioral responses to noxious stimuli and fear in glutamate receptor 5 (GluR5)- or GluR6-deficient mice. *J. Neurosci.* **25**, 977–984 (2005).
41. Burnashev, N., Villarroel, A. & Sakmann, B. Dimensions and ion selectivity of recombinant AMPA and kainate receptor channels and their dependence on Q/R site residues. *J. Physiol. (Lond.)* **496**, 165–173 (1996).
42. Bowie, D. & Mayer, M.L. Inward rectification of both AMPA and kainate subtype glutamate receptors generated by polyamine-mediated ion channel block. *Neuron* **15**, 453–462 (1995).
43. Wilding, T.J., Zhou, Y. & Huettner, J.E. Q/R site editing controls kainate receptor inhibition by membrane fatty acids. *J. Neurosci.* **25**, 9470–9478 (2005).
44. Koike, M., Iino, M. & Ozawa, S. Blocking effect of 1-naphthyl acetyl spermine on Ca^{2+}-permeable AMPA receptors in cultured rat hippocampal neurons. *Neurosci. Res.* **29**, 27–36 (1997).
45. Humeau, Y., Shaban, H., Bissiere, S. & Lüthi, A. Presynaptic induction of heterosynaptic associative plasticity in the mammalian brain. *Nature* **426**, 841–845 (2003).
46. Rodrigues, S.M., Bauer, E.P., Farb, C.R., Schafe, G.E. & LeDoux, J.E. The group I metabotropic glutamate receptor mGluR5 is required for fear memory formation and long-term potentiation in the lateral amygdala. *J. Neurosci.* **22**, 5219–5229 (2002).
47. Humeau, Y. *et al.* Dendritic spine heterogeneity determines afferent-specific Hebbian plasticity in the amygdala. *Neuron* **45**, 119–131 (2005).
48. Harvey, C.D. & Svoboda, K. Locally dynamic synaptic learning rules in pyramidal neuron dendrites. *Nature* **450**, 1195–1200 (2007).
49. Paré, D. & Collins, D.R. Neuronal correlates of fear in the lateral amygdala: multiple extracellular recordings in conscious cats. *J. Neurosci.* **20**, 2701–2710 (2000).

ONLINE METHODS

Electrophysiological recordings. Coronal brain slices containing the amygdala (300 µm thick, from −2.5 to −3.3 mm bregma) were prepared from 3–4-week-old Sprague-Dawley rats with a vibratome. Slices were continuously superfused in solution containing 119 mM NaCl, 2.5 mM KCl, 2.5 mM $CaCl_2$, 1 mM $MgSO_4$, 1.25 mM NaH_2PO_4, 26 mM $NaHCO_3$, 10 mM glucose and 0.05 mM picrotoxin (unless noted otherwise) and equilibrated with 95% O_2 and 5% CO_2 (pH 7.3–7.4) at 31–32 °C (unless indicated otherwise). Whole-cell recordings of EPSCs and EPSPs were obtained from principal neurons in the lateral amygdala under visual guidance (infrared differential interference contrast optics) with an EPC-9 amplifier and Pulse v8.30 software (HEKA Electronik). Synaptic responses were evoked by stimulation of the fibers in either the external capsule (cortical input) or the internal capsule (thalamic input). The patch electrodes (3–5 MΩ resistance) contained 150 mM potassium gluconate, 5 mM NaCl, 1 mM $MgCl_2$, 0.2 EGTA, 10 mM HEPES, 2 mM MgATP and 0.6 mM NaGTP (adjusted to pH 7.25 with KOH, 290 mOsm). For the *I-V* relationship experiments, cesium methanesulfonate was used instead of potassium gluconate and 20 mM TEA and 0.2–0.5 mM spermine were added to the pipette solution. In the perforated patch-clamp experiments, nystatin stock solution (30 mg ml^{-1} in DMSO) was freshly made every 3 h and added to the recording pipette solution (100–150 µg ml^{-1}). After obtaining a giga-seal, the input and series resistance decreased gradually until they reached the steady-state levels (normally within 30 min). Recording baseline EPSCs was started once the series resistance decreased to less than 20 MΩ. The perforated patch recording was terminated if a sudden decrease in the series resistance occurred, which is indicative of the patch rupture. Synaptic responses were filtered at 1 kHz and digitized at 2.5 kHz. To evoke synaptic responses, square current pulses (50–150 µA, 100-µs duration) were applied through concentric stimulating electrodes that consisted of silver-painted patch pipettes filled with the external solution. Membrane potential was held constant at −70 mV throughout the experiments in voltage-clamp mode unless indicated otherwise. Baseline EPSCs were evoked by stimulation of cortical or thalamic inputs every 20 s. During the baseline recording, the TSt was applied 10 s after the prior CSt. The standard ITDP induction protocol consisted of the paired TSt-CSt stimulation with the specified interval between TSt and CSt stimuli for 90 s at a 1-Hz frequency. In ITDP experiments, the stimulus intensity was adjusted to evoke synaptic responses with the amplitudes that were ~20–25% of the maximum amplitude response. Summary LTP graphs were constructed by normalizing data in 60-s epochs to the mean value of the baseline EPSC or EPSP. We obtained pharmacological reagents from Sigma (picrotoxin, nitrendipine, atropine, BAPTA, nystatin, spermine, ATP and GTP), Tocris Bioscience (D-AP5, DL-TBOA, ATPA, (S)-DHPG, NBQX, ryanodine, CPCCOEt, MPEP, LY 367385, SIB 1757, SYM2206, UBP 296, UBP 302, ACET, NASPM, TEA and MNI-glutamate), Enzo Life Sciences (Xestospongin-C) and Invitrogen (Alexa 594 and Fluo-5F).

Two-photon imaging and two-photon glutamate uncaging. Two-photon laser-scanning microscopy was performed using an Ultima imaging system (Prairie Technologies), a titanium:sapphire Chameleon Ultra femtosecond-pulsed laser (Coherent) and 60× (0.9 NA) water-immersion infrared objective (Olympus) as previously described[50]. Fluorescent dyes Alexa Fluor 594 and Fluo-5F were loaded into the principal neurons of the LAn with the pipette solution containing 140 mM potassium methane-sulfonate, 8 mM NaCl, 1 mM $MgCl_2$, 10 mM HEPES, 5 mM MgATP, 0.4 mM NaGTP, 5 mM QX-314, 60 µM Alexa 594 (structural dye with red fluorescence) and 300 µM Fluo-5F (Ca^{2+}-sensitive dye with green fluorescence). Alexa 594 and Fluo-5F were excited with the laser pulses at 820 nm, and changes in both red and green fluorescence were measured simultaneously in line-scan mode (500 Hz) in spine heads on an application of the uncaging pulse or electrical stimulation of cortical input to the LAn. Line scans were analyzed as changes in green (Fluo-5F) fluorescence normalized to red (Alexa Fluor 594) fluorescence (ΔG/R). Three to five traces of ΔG/R were averaged and smoothed with the Savitzky-Golay filter (2.4-ms window). In glutamate uncaging experiments, MNI-glutamate in the external solution was uncaged using the TriggerSync software (Prairie Technologies), and 0.2–0.5-ms pulses were delivered from a second titanium:sapphire Chameleon Ultra femtosecond-pulsed laser at 720 nm. The pulses were applied at a single point near the head of dendritic spine. Picrotoxin (50 µM) and SYM2206 (100 µM) were added to the artificial cerebrospinal fluid to inhibit $GABA_A$ receptors and AMPARs, respectively. To increase the chance of finding dendritic spines responding to electrical stimulation or uncaged glutamate, we used the external solution with a low concentration of Mg^{2+} (0–0.2 mM), which allowed NMDAR activation and detection of resultant Ca^{2+} transients in response to single stimuli.

Behavior. On the training day, the animal was placed in the conditioning chamber for 2 min before the onset of the conditioned stimulus (CSa), a tone that lasted for 30 s (5 kHz, 75 dB). The last 2 s of the CSa were paired with the UCS, 0.6 mA of continuous foot shock. After an additional 30 s in the chamber, the rat was returned to its home cage. Rats were tested at 48 h after training. For testing, rats were placed in a novel environment (cage) in which the tone (60 s) that had been presented during training was given after a 1-min habituation period. Freezing scores were calculated as the fraction (percentage) of the total CSa duration in which the rat remained immobile (frozen). Prior to behavioral training, rats were assigned randomly to one of three groups: CSa-UCS (paired), CSa alone and behaviorally naive. Rats in the paired group were trained and tested, as described above. Rats in the CSa alone group were trained and tested similarly to those of the paired group except that the foot shock UCS was omitted during training. Rats in the naive group were handled, but not exposed to the CSa or the UCS. Immediately after the conclusion of the test session, rats were used for electrophysiological recordings. The experimenters who completed the recordings were blind to the behavioral status of the animals.

Surgery and microinfusions. Male Sprague-Dawley rats weighing 350–375 g were housed in groups of four per cage for 2 weeks before surgery. They were maintained on a 12-h light/dark cycle (lights on at 07:00 a.m.) with food and water continuously available. Prior to surgery, each rat was anesthetized with sodium pentobarbital (65 mg per kg of body weight, intraperitoneal injection; Abbott Laboratories) supplemented with subcutaneous atropine (0.25 mg per kg, Sigma) to minimize bronchial secretions, and immobilized in a stereotaxic instrument with blunted earbars (David Kopf Instruments). Rats were implanted bilaterally with two stainless steel guide cannulae (26-gauge, Plastics One) with an internal dummy stylet extending 1.5 mm beyond the guide cannula tip aimed at the lateral amygdala nucleus (−2.8 mm caudal to bregma, ±5.0 mm lateral to midline, and −5.9 mm ventral to dura). The cannulae were fixed in place with skull screws and dental cement. Following surgery, the rats were housed singly. The dummy stylets were removed for infusions 1 week later and the animals received bilateral intra-amygdala infusions of either vehicle (70% DMSO) or the selective GluR5 KAR antagonist UBP 302 (Tocris) via a syringe pump and Hamilton syringes connected to polyethylene tubing, which was fitted to an injector stylette (30-gauge, Plastics One) extending 1.5 mm beyond the end of the cannula. UBP 302 was dissolved in 70% DMSO at a concentration of 10 µg $µl^{-1}$ and all animals received infusions at a rate of 0.1 µl min^{-1} for 3 min (total dose = 3 µg per side). Injectors were left in place for 2 min following the completion of infusions to allow for diffusion of the infusate. Animals were placed in a holding cage and, after 10 min, the rats were fear conditioned (they received two CSa-UCS pairings) and tested at 48 h post-training, as described above. The positions of the infusion cannulae were verified with Nissl stain in coronal brain sections through the amygdala. All animal procedures were approved by Mclean Hospital's Institutional Animal Care and Use Committee.

Statistical analysis. Data are presented as means ± s.e.m. Where appropriate, two-tailed Student's *t* test (paired or unpaired) was used for statistical analysis. For comparing more than two different groups, as in **Figure 8**, one-way ANOVA with Bonferroni's simultaneous multiple comparisons was used. The Mann-Whitney *U* test was used to compare freezing between vehicle- and UBP302-injected rats in **Supplementary Figure 14**. Statistical analysis was performed with Minitab15 software (Minitab), and $P < 0.05$ was considered to be statistically significant.

50. Richardson, R.J., Blundon, J.A., Bayazitov, I.T. & Zakharenko, S.S. Connectivity patterns revealed by mapping of active inputs on dendrites of thalamorecipient neurons in the auditory cortex. *J. Neurosci.* **29**, 6406–6417 (2009).